





LETTER | JULY 03 2024

Normal deformation of a soft lipid-based microtube in response to the flow generated by a tangential motion of a nearby microbead

Mohammad Doostaran ; Faegheh Hajizadeh  ; Ali Najafi 



Physics of Fluids 36, 071704 (2024)

<https://doi.org/10.1063/5.0215755>



APL Energy

Latest Articles Online!

Read Now



Normal deformation of a soft lipid-based microtube in response to the flow generated by a tangential motion of a nearby microbead

Cite as: Phys. Fluids **36**, 071704 (2024); doi: 10.1063/5.0215755

Submitted: 25 April 2024 · Accepted: 13 June 2024 ·

Published Online: 3 July 2024






View Online



Export Citation



CrossMark

Mohammad Doostaran,¹  Faegheh Hajizadeh,^{1,2,a)}  and Ali Najafi^{1,3,b)} 

AFFILIATIONS

¹Department of Physics, Institute for Advanced Studies in Basic Sciences (IASBS), Zanjan 45137-66731, Iran

²Optics Research Center, Institute for Advanced Studies in Basic Sciences (IASBS), Zanjan 45137-66731, Iran

³Research Center for Basic Sciences & Modern Technologies (RBST), Institute for Advanced Studies in Basic Sciences, Zanjan, Iran

^{a)} Author to whom correspondence should be addressed: hajizade@iasbs.ac.ir

^{b)} Electronic mail: najafi@iasbs.ac.ir

ABSTRACT

In this study, we experimentally examine the deformation of a micrometer-scale soft membrane in response to a periodic shear flow. We fabricate long and straight cylindrical-shaped soft microtubes from lipid bilayers as part of this study. A microtube with a diameter of about 1–5 μm is moved parallel to its longitudinal axes. At the same time, a polystyrene microbead, trapped by optical tweezers, is forced to stay near the external surface of the microtube. We study the induced shape deformation in the microtube for different shearing parameters. The effects related to the size of the bead, its distance to the surface of the microtube, and their relative speed are analyzed. The overall results qualitatively demonstrate the impact of shearing on the shape of the soft membrane.

Published under an exclusive license by AIP Publishing. <https://doi.org/10.1063/5.0215755>

The hydrodynamic effects associated with the flows near flexible surfaces and interfaces have long been the focus of classical studies in fluid dynamics.^{1–9} The flexibility of the walls enables them to undergo shape deformation in response to the motion of a nearby particle moving parallel to the interface. This softness of the interface and the membranes introduces nonlinearity into the problem. One immediate phenomenon corresponding to this shape deformation is the appearance of a normal force or flow component perpendicular to a flexible wall.¹⁰ Recently, there has been a renewed interest in exploring hydrodynamic-induced effects near walls,^{11–15} their potential applications,^{16,17} and possible relevance in biofluid mechanics.^{18,19} Although downscaling from macroscopic to microscopic experiments faced significant practical challenges due to the smallness of the induced deformations in the results compared to macro-scale experiments and the existence of thermal fluctuations of the membrane boundary at this scale,¹¹ studying this phenomenon at the micrometer-scale realm is important due to its relevance to numerous vital processes of flow patterns near biological membranes. The cell membrane and other lipid-bilayer structures living inside cells are flexible membranes that are continuously affected by hydrodynamic flows. Understanding the physics underlying the process of material transport in the confined

domain of living cells can help to develop efficient drug delivery systems.^{20,21}

In this study, we aim to experimentally investigate the hydrodynamic-mediated shape deformations in a micrometer-sized elastic membrane. To achieve this goal, we initially synthesized long and soft cylindrical shape microtubes from lipid bilayers in an aqueous media. The softness of these lipid bilayers can be attributed to their surface tension and bending rigidity.^{22,23} Subsequently, we employed optical tweezers to immobilize a polystyrene microbead and manipulate its motion in the vicinity of such a soft microtube. In this setup, we have control over the relative distance and speed between the microbead and the tube's surface. Furthermore, we examine the effects corresponding to the size of the microbead. We analyze the resulting shape deformation of the microtube's wall induced by the hydrodynamic shear flow. One significant practical challenge encountered when scaling down from macroscopic to microscopic experiments is the smallness of the induced deformations in the results, compared to the cases of macro-scale experiments.¹¹ Nevertheless, our experimental study qualitatively demonstrates that the deformation pattern of a microtube as a result of an applied local shear flow is well observable. We conclude our experimental study with a simplified scaling analysis

that brings an intuitive picture, showing how normal deformation can arise from a tangential shear.

In our experimental study, we want to investigate the response of a flexible wall to a local shear flow. In particular, we aim to observe how a bead moving parallel to a locally flat soft wall can result in normal stresses. Local deformations induced on the wall will be the experimental manifestation of such normal stresses. We prepare long and stiff microtubes from lipid bilayers. The surface of a microtube resembles a flexible membrane. In order to exert localized hydrodynamic shear force on the surface, one can consider a polystyrene bead that is forced to move adjacent and parallel to the surface. As the relative motion of the bead and the surface is important, we use an alternative method in which the microbead is fixed by optical tweezers and the tube is moving parallel to its longitudinal axes.

Figure 1(a) schematically shows the relative motion of an optically trapped microsphere near the upper boundary of a microtube. When the sample is shifted to the left relative to the trapped particle coordinate, the presence of the particle alters the stress profile of the fluid around it, causing deformation of the microtube. In each experiment, the particle is initially trapped and placed at the appropriate depth near the microtube where the microtube edge appears sharp. The microtube is laterally positioned at a specific distance, d , from the microbead. The sample chamber is then moved by a piezo stage, controlled by the computer. We applied a linear back-and-forth motion to the piezo stage. During each experiment, the piezo movement is adjusted so that the trapped particle and microtube experience a relative motion with constant speed. As seen from the Lab frame in which the microbead is fixed, the tube moves along its longitudinal axes. To measure the membrane's deformation accurately, we developed a program code for image processing to identify the membrane's edge pixels in recorded video frames, depicted as green lines in Figs. 1(b)–1(d) (Multimedia view). In all our experiments, we consistently observed a sinusoidal-like behavior just behind the bead, featuring both a minimum point and a maximum point. To ensure a fair comparison across all experiments analyzed under the same conditions, a portion of the pattern with the greatest deformation between two extremes, marked with Δ in Fig. 1(a), is fitted to a line. The slope of this line, denoted by α , serves as the foundation for our subsequent investigations.

In the following, we will present the results of the hydrodynamic-induced deformations of the tube. For more information about the microtube preparation and experimental setup, refer to the before the conclusion.

It is important to note that a variety of parameters significantly affect the deformation of the soft membrane. These parameters include temperature, the size of lipid microtubules, the size of microspheres, their relative velocity, and the relative distance between the microsphere and the membrane. In this study, we have employed a comparative method to examine the impact of some of these parameters. Specifically, in each experiment, we kept all parameters constant except for one, which we varied.

It should be noted that the optical gradient force, arising from the difference in refractive index between water and the membrane, has the potential to deform the freshly grown palmitoyl-2-oleoyl-sn-glycerol-3-phosphatidylcholine (POPC) membrane in water. To ensure that any observed and measured deformations in the membrane are solely due to hydrodynamic reasons and that the influence of optical forces can be disregarded, we conducted additional experiments. These

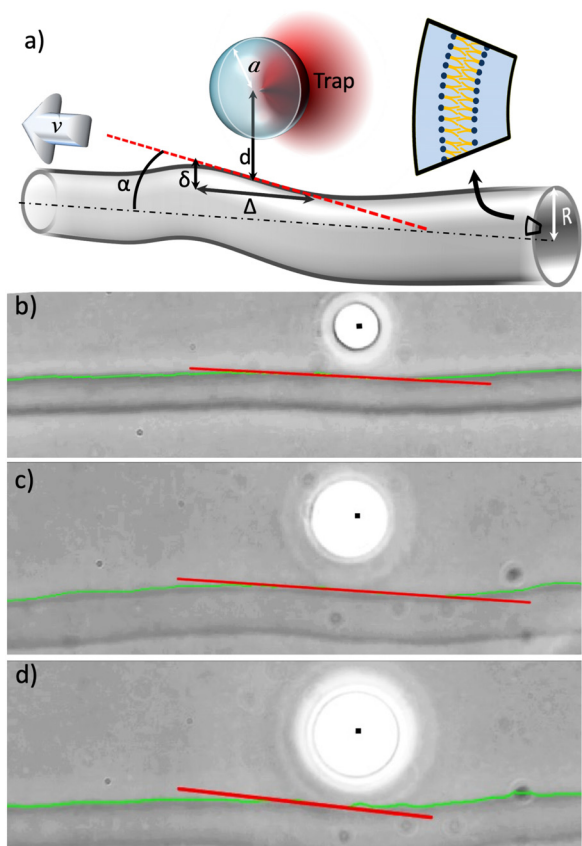


FIG. 1. (a) Schematic view showing the relative motion of an optically trapped microsphere near the upper boundary of a microtube. Note that the trapped particle remains stationary in the microscope's field of view while the microtube moves with respect to the particle. The radius and the relative speed of the bead are denoted by a and v , respectively. The deformed shape of the upper portion can be characterized by two parameters, Δ and δ , the longitudinal and lateral sizes of the deformed region. The local slope of the deformed wall can be given by $\alpha = \delta/\Delta$. (b)–(d) The microscopic images showing the hydrodynamic induced deformations on the surface of a flexible microtube. In each image, the motion of the piezo stage forces the microtube to move along its longitudinal axes from right to left. The trapped microsphere remains close to the microtube. The green curve represents the result of the image processing used to detect the near boundary of the microtube which is then fitted to a line (red) to obtain the slope. The center of the microsphere is shifted with respect to the center of the trapping laser focal spot (small black squares) due to the drag force. Multimedia available online.

experiments involved using an empty trap, varying laser power, and adjusting the distance from the membrane. As a result, we observed that the deformation caused by the gradient force is not visible at intensities lower than 40 mW and distances greater than $1 \mu\text{m}$ from the membrane to the center of the laser focal point within the chamber. Figure 2 shows a typical result of studying the effect of the presence of a moving trapped particle. As can be seen in this figure, when an empty trap is moved in the vicinity of a microtube, the measured slope shows a Gaussian distribution, which is the result of the thermal fluctuation of the membrane boundary. At this distance, the gradient force of the optical trap does not cause a specific deformation on the membrane. However, with the same velocity and distance, when there

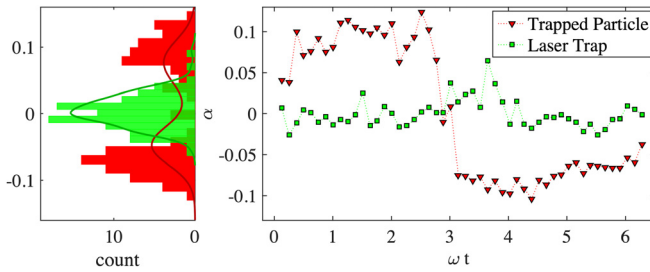


FIG. 2. The slope of the deformation of the boundary just behind the trapping point as a function of the piezo stage oscillating phase in an oscillatory motion near the membrane, along with the corresponding histogram. The slope of the deformation is measured by linearly fitting the near-boundary region of the membrane for a trapped particle (red triangle) and an empty trap (green square). The distance from the focal spot to the membrane as well as the oscillating velocity are held constant at $d = 3.8 \pm 0.4 \mu\text{m}$ and $v = 40 \mu\text{m/s}$, respectively, for both measurements, while the particle radius is $2a = 4.74 \mu\text{m}$. Each data point in the graph is an average of the measured slopes for two cycles of data.

is a particle in the trap, the graph of the slope shows a different deformation with a reverse direction of the slope and a distribution of the measured slope with two peaks.

After observing that an empty trap is not able to deform the tube, we proceed and investigate the different parameters that can affect the strength of the hydrodynamic shear force. Among different parameters, we concentrate on the distance between the bead and the tube, the size of the bead, and the relative speed of the bead and tube.

To study the effects of bead-tube separation, we choose a bead having a diameter of about $3.21 \mu\text{m}$ and a long microtube with a diameter of $2.9 \mu\text{m}$. Then, we repeat the shearing experiment for three different relative positions given by $d = 2.8, 4.3,$ and $6.8 \mu\text{m}$. Figure 3 shows the experimental results for the slope of the outer surface of the tube as a function of time. The results are presented for a single period of the relative motion of the tube and the bead. The angular frequency of the piezo stage displacement, ω , is used to make nondimensional time. In addition to the dynamical variations of the slope, we also plotted the histogram of the slope values. The histogram is calculated from the numerical data collected from two cycles of piezo stage motion.

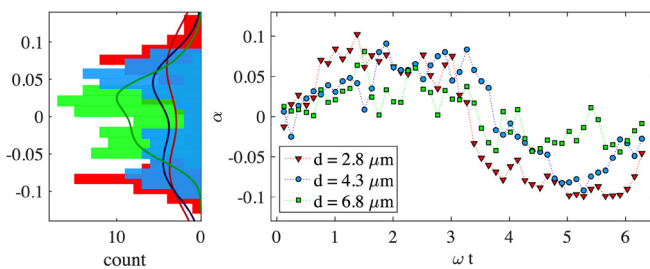


FIG. 3. The effect of the distance between the moving particle and the membrane: The slope of the deformation as a function of the piezo stage oscillating phase at a constant speed near the membrane, along with the corresponding histogram. The trapped particle size and the oscillating velocity are held constant at $2a = 3.21 \mu\text{m}$ and $40 \mu\text{m/s}$, respectively, while the distance from the focal spot and the membrane varies as $d = 2.8 \mu\text{m}$ (red triangle), $d = 4.3 \mu\text{m}$ (blue circle), and $6.8 \mu\text{m}$ (green square). The curves in the histogram graph represent the normal kernel function.

Some general features of the results in Fig. 3 can be distinguished. First, a form of symmetry in the results for the first and second half periods is expected to be observed. This is because the first and second half periods of the motion correspond to the same relative velocities of the bead and tube. This symmetry is reflected statistically both in the dynamical data of the slope and its histogram. The slope has the same maximum and minimum values within a complete cycle. This symmetry ensures that the tube moves along its axes. The second feature that is reflected in the time-dependent results for the slope is a relaxation behavior between the first and second half periods of the motion. At the end of the first half period of the motion, the piezo stage changes its motion abruptly from a right to a left-moving state. Owing to the dominance of viscous forces, the tube is not able to respond instantaneously and it will take time to achieve its steady state deformed shape. Some time-dependent processes related to the dynamical responses of the ambient fluid and the tube may contribute to this relaxation. We can clearly observe this relaxation time in our data. However, regarding our limit of accuracy, the results for relaxation time do not show any clear dependence on bead-tube separation.

The results in Fig. 3 show that the deformation pattern of the tube depends on the distance by which the bead and the tube are separated. A higher separation corresponds to a smaller slope. For a separation of $d = 2.8 \mu\text{m}$, the outer part of the tube experiences a slope of about $\alpha \approx 0.1$. This shows that a bead moving near a tube will produce much stronger normal stress on the tube in comparison with a bead moving at far distances.

The size of the bead and its relative speed (with respect to the tube) are two other main parameters that can affect the normal hydrodynamic stress exerted on the tube. Figures 4 and 5 show the dependence of deformation slope on bead size and its relative speed, correspondingly. Similar to Fig. 4, two features of symmetry and relaxation time can be apparently observed here. From a simple physical intuition, we expect to observe stronger hydrodynamic effects for large and fast-moving beads. Figure 4 shows that a bead having a radius of $2.37 \mu\text{m}$ induces a larger slope on the tube rather than what is induced by a bead having a diameter of about $1.09 \mu\text{m}$. Figure 5 shows the results of deformation for various relative speeds of the bead. Within our experimental precision, a relative resolution between different

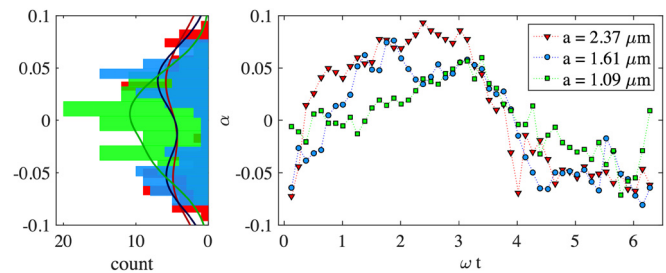


FIG. 4. The effect of particle size on the membrane deformation. The slope of the deformation as a function of the piezo stage oscillating phase, along with the corresponding histogram, in an oscillatory motion near the membrane. The distance between the focal spot and the membrane, as well as the velocity, is held constant at $d = 3.7 \mu\text{m}$ (average distance during a period) and $v = 40 \mu\text{m/s}$, respectively, while the particle size varies as $a = 2.37 \mu\text{m}$ (red triangle), $a = 1.61 \mu\text{m}$ (blue circle), and $a = 1.09 \mu\text{m}$ (green square). The curves in the histogram graph represent the normal kernel function.

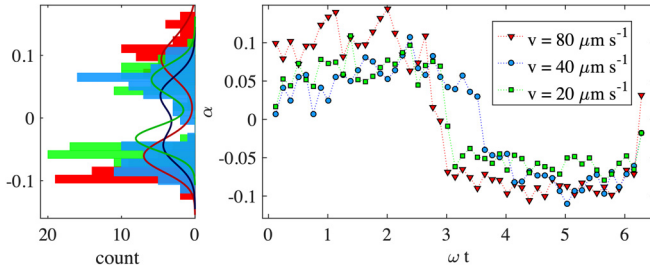


FIG. 5. The effect of the relative velocity between the moving microsphere and the membrane on the deformation: The slope of the deformation as a function of the piezo stage oscillating phase, along with the corresponding histogram, in an oscillating motion near the membrane. The distance between the focal spot and the membrane, as well as the particle size, is held constant at $d = 3.5 \mu\text{m}$ average distance during a period and $2a = 4.74 \mu\text{m}$, respectively, while the piezo velocity varies as $v = 80 \mu\text{m/s}$ (red triangle), $v = 40 \mu\text{m/s}$ (blue circle), and $v = 20 \mu\text{m/s}$ (green square). The curves in the histogram graph represent the normal kernel function.

speeds can be seen. As it is expected, higher relative speeds can induce a relatively larger deformation.

After presenting our experimental results, we present a theoretical insight to address the physical mechanism behind membrane deformation in the following paragraphs. The complicated geometry of a solid sphere moving near an elastic tube does not allow for obtaining an analytic solution to the corresponding elastohydrodynamic problem. To have a qualitative understanding of what happens when a solid body is moving near a soft wall, we consider a simplified geometry in which a very small and solid sphere moves near a locally flat and soft wall. Consider a rigid sphere with radius a moving with velocity v , parallel to a soft wall having tension γ and bending rigidity κ . Let us assume that the membrane is initially flat and the center of the sphere has a distance d from the undeformed wall. We denote by η and ρ , the viscosity and density of the ambient fluid. For our purpose, the Reynolds number, the ratio of inertia to viscosity, which is denoted by $\text{Re} = \rho va/\eta$, is small. Hence, the governing equations for the fluid flow reads as²⁴

$$\eta \nabla^2 \mathbf{u} - \nabla p = 0, \quad \nabla \cdot \mathbf{u} = 0, \quad (1)$$

where \mathbf{u} and p stand for velocity and pressure field in the fluid. The velocity field should be subjected to the convenient boundary conditions. At the steady state where all fields are time-independent, the velocity on the sphere is given by v and it should vanish on the soft wall. Furthermore, the component of the stress tensor should obey the continuity rules on the soft wall. More importantly, the normal component of the stress tensor should be balanced by the elastic forces of the wall. These elastic forces depend on elastic parameters like γ and κ and also they depend on the deformation pattern of the wall. This will result in a nonlinear coupling between the flow and the shape of the wall. The steady-state and instantaneous solution to the above-mentioned equations show that a moving sphere near a soft wall requires an inevitable deformed shape for the elastic wall. Denoting by $z = \zeta(x, y)$, the deformed shape of the membrane in Monge representation, it will satisfy the following differential equation:^{10,11}

$$(\gamma \nabla^2 - \kappa \nabla^4) \zeta(x, y) = \frac{6}{5} \eta v_{\parallel} \frac{r \ell^4}{h^2 (r^2 + \ell^2)^2} \cos \phi, \quad (2)$$

where $r = \sqrt{x^2 + y^2}$, $\ell = \sqrt{2a(d-a)}$, and ϕ shows the polar angle in the xy -plane. The expression at the right-hand side of the

above-mentioned equation stands for the pressure distribution corresponding to a moving sphere near a soft and flat wall. A dimensional argument is useful to gain insight into the solutions of the above differential equation. As a result of azimuthal dependence, $\cos \phi$, asymmetric deformation of the membrane is expected to be observed. A trough in the membrane just in front of the sphere ($\phi = 0$) and a peak at the backward direction ($\phi = \pi$) are the main geometrical features of the deformed membrane. In a qualitative picture, similar to what is depicted in Fig. 1(d), we denote the extent of normal and lateral deformations of the membrane by δ and Δ . Here, Δ shows how far the trough and the peak are apart on the membrane, and δ is simply the height of the peak. The right-hand-side of Eq. (2) shows that ℓ is a length scale over which the stresses from the fluid acting on the membrane relax to zero. This will naturally result in the extent of the lateral deformation of the membrane being about $\Delta \sim \ell$. Putting this result into Eq. (2) as $\nabla \sim \ell^{-1}$, $r \sim \ell$ and neglecting the term proportional to γ , we obtain $\delta \sim (\eta v/\kappa) a^{\frac{5}{2}} d^{\frac{1}{2}}$. Just behind the sphere, the membrane has a maximum slope in the polar direction $\phi = 0$ that is given by $\alpha \sim \delta/\Delta$. This slope can be written as

$$\alpha \sim \frac{\eta v a^2}{\kappa} \left(1 + \mathcal{O}\left(\frac{a}{d}\right) \right). \quad (3)$$

Two considerations can help us to adapt this result for the case of a bead moving near a tube. First, note that the geometry of a tube introduces a new length scale R , the diameter of the tube, into the problem. Also one may argue that the stiffness of a part of a lipid tube is not necessarily the same as the stiffness of a flat layer. Regarding these considerations, we can write a dimensional relation for the slope as

$$\alpha = \frac{\eta v a^2}{\kappa_{\text{eff}}} f\left(\frac{a}{d}, \frac{d}{R}\right), \quad \frac{a}{d} \ll 1 \quad \text{and} \quad \frac{d}{R} \ll 1, \quad (4)$$

where the effective stiffness is denoted by κ_{eff} and dimensionless function $f(x, y)$ is used to take into account the role of different length scales. For a typical experiment presented in Fig. 3, the relative speed is about $v \sim 40 \mu\text{m/s}$, the size of the bead is about $a \sim 3 \mu\text{m}$, and $a/d \sim 1$. Using the viscosity of water that is given by $\eta \sim 10^{-3} \text{Pa} \cdot \text{s}$ and considering the rigidity as $\kappa_{\text{eff}} \sim 1000 k_B T$,¹⁵ we will obtain an estimation for the slope as $\alpha \sim 10^{-1}$. This demonstrates that our scaling analysis offers a comparable prediction to the experimental data.

In the above-mentioned dimensional analysis, for simplicity, we focused on bending rigidity and ignored the role of tension. Since our experimental analysis does not provide any insight into the role of the membrane's bending or shear elasticity, the above-mentioned analysis can be considered a naive picture. It should be noted that a previous theoretical study has concluded that for the motion of a sphere in the centerline of an elastic tube,²⁵ in-plane shear elasticity of the membrane dominates over the bending mode.

In the following paragraphs, we will explain the microtube preparation and experimental setup to produce soft and long microtubes, resembling elastic membranes, we adopted the commonly used method of vesicle production from water-immersed lipid bilayers, with some modifications. Contrary to the previous report where long microtubes were produced by stretching vesicles using elongation flow,²⁶ the method proposed here involves bud formation in the presence of liquid flow, leading to microtube formation along the flow. Initially, the desired lipid is dissolved in an appropriate organic solvent, such as chloroform or methanol, to create a lipid solution. Subsequently, the solvent is gently evaporated using a nitrogen gas stream or lyophilization (freeze-drying)

to form a thin lipid film on the container walls. In this study, to create a microtube, the coverglass, serving as the substrate for the lipid film, is initially washed. Then, the lipid-concentrated solution, palmitoyl-2-oleoyl-sn-glycerol-3-phosphatidylcholine (POPC) purchased from Avanti Polar Lipids, is applied to the cleaned cover glass in a narrow line [Fig. 6(a)].

The sample chamber is constructed using the same coverglass and a microscope slide, which is spaced apart by a narrow strip of double-stick Scotch tape. The chamber, shown in Fig. 6(a), is prepared by creating entrance and exit apertures for the flow of the aqueous mixture onto the lipid coat. It is filled with a mixture of water and suspended polystyrene microparticles, where a gentle water flow aids in the budding process. This facilitates the accumulation of a significant number of budding bubbles at the water–lipid interface. The pressure gradient of water from the entrance to the exit of the chamber creates a flow that stretches some of these lipid bilayer bubbles along the fluid flow within the fabricated chamber. These stretched lipid bilayer bubbles eventually form tubular, soft lipid bilayers that have grown along the water flow. The flow creates a pressure gradient from the entrance to the exit of the chamber, resulting in the stretching of some lipid bilayer bubbles along the flow. These stretched lipid bilayer bubbles eventually form soft tubular structures that grow parallel to the water flow within the fabricated chamber.

Figure 7(a) shows the process of microtube growth under the microscope. The images, from left to right, show the boundary of the lipid layer where there is no flow, flow causing membrane buds to form, and then microtubes being formed along the flow. The flow direction in these images is from bottom to top. Observations indicate that the microtubes grow on a lipid coating with average flow velocities higher than a few hundred micrometers per second. Once the microtubes grow sufficiently, the entrance and exit of the chamber are blocked using silicone glue, preventing any pure flow that can be observed through microsphere fluctuation. Although the inlet and outlet are fully closed, a gradual shrinking process can still be observed in the stretched tubular POPC lipid bilayer. The rate of contraction of microtubes varies at different points along the length of microtubes and also varies between microtubes. On average, the contraction speed is a few micrometers per second. However, when it comes to long microtubes (over a few tens of micrometers) near their growth site, the contraction speed is observed to be significantly slower for several minutes, with minimal changes in their diameter and length.

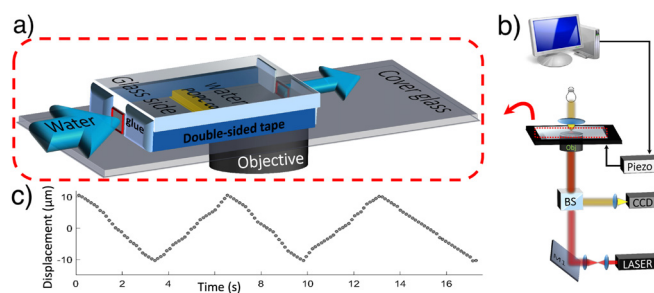


FIG. 6. (a) The sample chamber is used for producing microtubes and measuring deformation. The sample chamber was used in conjunction with an optical tweezers setup, which is shown schematically in (b). (c) The displacement of the center of mass of a microspheres attached to the cover glass moved in a triangular manner by a piezo stage controller with constant velocity.

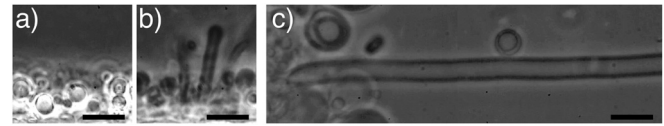


FIG. 7. The process of microtube growth as observed under the microscope shown from left to right: (a) formation of buds in the presence of water flow, (b) microtube formation along the flow, and (c) a long and straight cylindrical-shaped soft microtubes from lipid bilayers.

To manipulate a microparticle near the membrane, we utilized the optical tweezers setup. The optical tweezers setup used here [Fig. 6(b)] is based on an inverted microscope (Olympus, IX-71) and is similar to that described in Ref. 27. An expanded continuous wave laser beam (Nd-YAG, Compass, Coherent, $\lambda = 1064$ nm) is introduced to the optical path of the microscope through its side port. A phase contrast objective lens ($100\times$, Olympus, NA = 1.3, Ph3) focuses the laser beam into the sample chamber. The sample chamber is mounted on a 2D piezo stage (Physik Instrumente, PI-527.2 cl), which provides 2D positioning of the floated microtube relative to a trapped micro bead with nanometer resolution. Colloidal solutions of polystyrene (PS) beads with mean diameters of 2.18, 3.21, and $4.74\ \mu\text{m}$, were highly diluted in distilled water. The laser power was 35 mW at the sample. We applied a linear back-and-forth motion to the piezo stage. As a function of time, the displacement of the stage shows a symmetric triangular pattern. To demonstrate this linear motion of the piezo stage with time, we attached a particle to the cover glass and moved it in a triangular manner. The movement of the particle's center of mass due to the piezo is shown in Fig. 6(c). The speed of this motion can be expressed in terms of the amplitude of displacement and the durations of a half-cycle period of the triangular pattern denoted by π/ω . The maximum displacement of the piezo stage during this triangular motion near the membrane is 20 micrometers. The videos capturing these movements are recorded at 50 frames per second using a CCD camera (Pixelink, PL-B761U).

In conclusion, we conducted a series of experiments to demonstrate how a shear flow can deform a soft wall. In our experiments, the shear flow is produced by a polystyrene bead that is forced to move relative to the surface of a soft microtube. Our experiments qualitatively show that the normal deformation induced on the surface of a lipid microtube can be adjusted by the strength of the shear flow. Due to practical difficulties that limited our precision, we were not able to go beyond the qualitative picture. In addition to the normal deformation of a soft wall, the normal force on a bead moving near a soft wall is the subject of our interest. We hope to measure such normal force in our future works.

The authors thank Farshid Mohammad Rafiee for his helpful discussion.

AUTHOR DECLARATIONS

Conflict of Interest

The authors have no conflicts to disclose.

Author Contributions

Mohammad Doostaran: Conceptualization (equal); Data curation (equal); Formal analysis (equal); Investigation (equal); Resources

(equal); Software (equal); Validation (equal); Writing – original draft (equal). **Faegheh Hajizadeh:** Conceptualization (equal); Funding acquisition (equal); Project administration (equal); Resources (equal); Supervision (equal); Validation (equal); Visualization (equal); Writing – original draft (equal); Writing – review & editing (equal). **Ali Najafi:** Conceptualization (equal); Funding acquisition (equal); Methodology (equal); Project administration (equal); Supervision (equal); Validation (equal); Visualization (equal); Writing – original draft (equal); Writing – review & editing (equal).

DATA AVAILABILITY

The data that support the findings of this study are available from the corresponding authors upon reasonable request.

REFERENCES

- ¹K. Aderogba and J. Blake, “Action of a force near the planar surface between two semi-infinite immiscible liquids at very low Reynolds numbers,” *Bull. Aust. Math. Soc.* **18**, 345–356 (1978).
- ²I. Berdan and C. L. G. Leal, “Motion of a sphere in the presence of a deformable interface,” *J. Colloid Interface Sci.* **87**, 62–80 (1982).
- ³A. Daddi-Moussa-Ider, M. Lisicki, and S. Gekle, “Mobility of an axisymmetric particle near an elastic interface,” *J. Fluid Mech.* **811**, 210–233 (2017a).
- ⁴B. Saintyves, T. Jules, T. Salez, and L. Mahadevan, “Self-sustained lift and low friction via soft lubrication,” *Proc. Natl. Acad. Sci. U. S. A.* **113**, 5847–5849 (2016).
- ⁵A. Daddi-Moussa-Ider and S. Gekle, “Hydrodynamic mobility of a solid particle near a spherical elastic membrane: Axisymmetric motion,” *Phys. Rev. E* **95**, 013108 (2017).
- ⁶A. Farutin, T. Biben, and C. Misbah, “3D numerical simulations of vesicle and inextensible capsule dynamics,” *J. Comput. Phys.* **275**, 539–568 (2014).
- ⁷L. J. Fauci and A. McDonald, “Sperm motility in the presence of boundaries,” *Bull. Math. Biol.* **57**, 679–699 (1995).
- ⁸R. Ledesma-Aguilar and J. M. Yeomans, “Enhanced motility of a microswimmer in rigid and elastic confinement,” *Phys. Rev. Lett.* **111**, 138101 (2013).
- ⁹Z. Zhang, V. Bertin, M. Arshad, E. Raphael, T. Salez, and A. Maali, “Direct measurement of the elastohydrodynamic lift force at the nanoscale,” *Phys. Rev. Lett.* **124**, 054502 (2020).
- ¹⁰S. Nezamipour and A. Najafi, “Flow pumping by external periodic shear applied to a soft interface,” *Sci. Rep.* **11**, 15041 (2021).
- ¹¹B. Rallabandi, N. Oppenheimer, M. Y. Ben Zion, and H. A. Stone, “Membrane-induced hydroelastic migration of a particle surfing its own wave,” *Nat. Phys.* **14**, 1211–1215 (2018).
- ¹²C. Kurzthaler, R. Brandão, O. Schnitzer, and H. A. Stone, “Shape of a tethered filament in various low-Reynolds-number flows,” *Phys. Rev. Fluids* **8**, 014101 (2023).
- ¹³D. L. Chase, C. Kurzthaler, and H. A. Stone, “Hydrodynamically induced helical particle drift due to patterned surfaces,” *Proc. Natl. Acad. Sci. U. S. A.* **119**, e2202082119 (2022).
- ¹⁴A. Kargar-Estahbanati and B. Rallabandi, “Lift forces on three-dimensional elastic and viscoelastic lubricated contacts,” *Phys. Rev. Fluids* **6**, 034003 (2021).
- ¹⁵V. Sharma, F. Fessler, F. Thalmann, C. M. Marques, and A. Stocco, “Rotational and translational drags of a Janus particle close to a wall and a lipid membrane,” *J. Colloid Interface Sci.* **652**, 2159–2166 (2023).
- ¹⁶S. Hazra, S. Mitra, and A. K. Sen, “Migration and spreading of droplets across a fluid–fluid interface in microfluidic coflow,” *Langmuir* **38**, 9660–9668 (2022).
- ¹⁷N. Xue, J. K. Nunes, and H. A. Stone, “Shear-induced migration of confined flexible fibers,” *Soft Matter* **18**, 514–525 (2022).
- ¹⁸J. B. Grotberg, “Respiratory fluid mechanics and transport processes,” *Annu. Rev. Biomed. Eng.* **3**, 421–457 (2001).
- ¹⁹J. B. Grotberg and O. E. Jensen, “Biofluid mechanics in flexible tubes,” *Annu. Rev. Fluid Mech.* **36**, 121–147 (2004).
- ²⁰F. Yuan, C. Yang, and P. Zhong, “Cell membrane deformation and bioeffects produced by tandem bubble-induced jetting flow,” *Proc. Natl. Acad. Sci. U. S. A.* **112**, E7039–E7047 (2015).
- ²¹D. Huber, A. Oskooei, X. Casadevall i Solvas, A. deMello, and G. V. Kaigala, “Hydrodynamics in cell studies,” *Chem. Rev.* **118**, 2042–2079 (2018).
- ²²W. Helfrich, “Elastic properties of lipid bilayers: Theory and possible experiments,” *Z. Naturforsch. c* **28**, 693–703 (1973).
- ²³H. Duwe, J. Kaes, and E. Sackmann, “Bending elastic moduli of lipid bilayers: Modulation by solutes,” *J. Phys.* **51**, 945–961 (1990).
- ²⁴L. D. Landau and E. M. Lifshitz, *Fluid Mechanics*, 2nd ed., Course of Theoretical Physics, Vol. 6 (Pergamon, 1987).
- ²⁵A. Daddi-Moussa-Ider, M. Lisicki, and S. Gekle, “Hydrodynamic mobility of a sphere moving on the centerline of an elastic tube,” *Phys. Fluids* **29**, 111901 (2017b).
- ²⁶V. Kantsler, E. Segre, and V. Steinberg, “Critical dynamics of vesicle stretching transition in elongational flow,” *Phys. Rev. Lett.* **101**, 048101 (2008a).
- ²⁷M. H. Khosravi, V. Shahabadi, and F. Hajizadeh, “Microsphere-coupled optical tweezers,” *Opt. Lett.* **46**, 4124–4127 (2021).